Journal of Power Sources 180 (2008) 859–863

Contents lists available at ScienceDirect

Journal of Power Sources

journal homepage: www.elsevier.com/locate/jpowsour

Short communication

SnSb micron-sized particles for Li-ion batteries

L. Simonin*, U. Lafont, E.M. Kelder

Laboratory for Nano-Structured Materials, Department of Chemical Technology, Faculty of Applied Sciences, Delft University of Technology, Julianalaan 136, 2628 BL, Delft, The Netherlands

ARTICLE INFO

Article history:
Received 14 December 2007
Received in revised form 1 February 2008
Accepted 9 March 2008
Available online 14 March 2008

Keywords:
Li-ion battery
Alloy
SnSb
Micron-sized particles
Post-mortem TEM
Negative electrode

ABSTRACT

Micrometre-sized particles of Sn/SnSb were produced with a simple technique consisting in melting commercial ingots of tin and antimony separately at 280 °C and 680 °C, respectively, and casting them together in a ceramic boat. The solid alloy was then crushed into a homogeneous powder by grinding and sieving. The obtained powder was characterised by X-ray diffraction, and electron microscopy. Elemental and phase composition analyses were performed via, inductive coupled plasma and differential scanning calorimetry, respectively. The material was further tested as electrode material in a lithium galvanic cell. It showed relatively good capacity retention for at least 15 cycles. TEM analysis on post-mortem electrode samples showed the formation of nanostructures after the first discharge followed by a progressive disappearance of the micron-sized particles upon further cycling. Fading at higher cycles is explained by the formation of isolated metallic nano-particles that become inactive for further storage of lithium.

1. Introduction

It is well known that intermetallics and metallic alloys are of great interest for replacing carbon materials as anodes in Li-ion batteries, because of their high gravimetric capacity [1–3]. However, it is well admitted that an enormous capacity loss upon cycling is partly due to the huge volume changes as a result of the displacement reactions taking place during charge and discharge. These displacement reactions induce cracks which lead to contact loss and hence an electrical impedance rice, resulting in power loss [2]. Nevertheless, in order to limit or to avoid this drawback, one of the most common approaches is to use intermetallic compounds with an inert metal (e.g. Cu, Co, Ni, etc.) as a buffering matrix with an active metal (e.g. Si, Sn, Sb, etc.) [4–6]. In case of an optimised system, the matrix also accepts lithium for storage, but then at different potentials. Hence, one component reacts with lithium while the other one acts as a buffer at the same time. As soon as the first active component is fully lithiated, the second one accepts lithium and then the first one acts as the buffer. This approach has been studied in the case of Si/C composites [7,8], as well as for SnSb [9–17]. This latter case will also be the subject of the work described here.

Several synthesis techniques have been used to prepare SnSb or Sn/SnSb compounds, e.g. reductive precipitation, high energetic ball milling, and carbothermal reduction. Reductive precipitation normally uses metal chlorides as precursors and $NaBH_4$ [9–13] or zinc powder [12] as reductive agent. High energetic ball milling under inert atmosphere [14] of the individual metals also leads to a desired composition. Both techniques typically result in the formation of sub-micron or nano-crystalline materials. In contrast, micro-crystalline powders are usually fabricated by annealing under inert atmosphere of elemental powders [13,15] or by carbothermal reduction of metal oxides [16]. The method to produce micro-crystals used in this study is based on a very well-known and actually old melting process of casting of molten metals, followed by grinding and sieving. This leads to the formation of particles in the order of tens of a micrometre. Often an agglomerate is defined as a conglomeration of particles, and then the particles as a constitution of one or more crystallites, with the crystallites similar to domains and grains, i.e. in X-ray diffraction (XRD) the main diffracting regimes. Usually, melt casting does not give any agglomerates, so that upon ball milling only particles can be found. It will be shown that applying this method to form intermetallic material provides materials with similar properties as made with methods that have been described above. These particles then were characterised with different techniques: X-ray diffraction, scanning electron microscopy (SEM), differential scanning calorimetry (DSC) and inductively coupled plasma-optical emission spectroscopy (ICP-OES). The electrochemical behaviour of the material was investigated via galvanostatic tests. Finally, post-mortem analysis was performed using transmission electron microscopy of samples measured after 1, 15 and 100 charging and discharging cycles.

* Corresponding author. Tel.: +31 15 278 5536; fax: +31 15 278 4945.
E-mail address: l.simonin@tudelft.nl (L. Simonin).

0378-7753/$ – see front matter © 2008 Elsevier B.V. All rights reserved.
doi:10.1016/j.jpowsour.2008.03.014

2. Experiments

2.1. Synthesis

Tin and antimony metal ingots were used in a 1:1 molar ratio in order to form the SnSb intermetallic compound. The two metals were molten separately in carbon crucibles 50 °C above their melting points, i.e. antimony was heated up to 680 °C while tin was heated up to 280 °C. Both metals were then cast in the same ceramic boat. It is further emphasised that the temperatures of the liquid metals was chosen such that when mixed the mixture is still a liquid. This can be seen by using phase diagram (Fig. 1) and the heat capacities of Sn and Sb, i.e. 31.4 J mol^{-1} K^{-1} and 29.1 J mol^{-1} K^{-1}, respectively. The heat capacities are almost the same as well as the densities (6.7 for Sb and 7.2 for Sn). Hence, by mixing these liquids, one may expect a final temperature of the average of both. When looking in the phase diagram, at this temperature, the system is then still a liquid. The obtained mixture was then cooled down to room temperature. According to the phase diagram, the SnSb intermetallic phase would precipitate starting at 424 °C. Also, the phase diagram shows that the SnSb phase could accept a little more Sn as well as Sb. The obtained ingots were later crushed to obtain a powder by grinding followed by sieving with a 45-μm sieve. Parts of the crushed sample were annealed at 300 °C for 60 h in order to reduce the impurity phases.

2.2. Composition and morphology

The microstructure and texture of the powders were analysed via SEM with a "Philips XL20" microscope and with TEM on a Philips CM30T electron microscope with a LaB_6 filament as electron source operating at 300 kV. Furthermore, the powder was analysed by XRD with a "Bruker-AXS Diffractplus D8" diffractometer operating with Cu Kα radiation. The elemental composition of the alloy was then measured by ICP-OES using a PerkinElmer Optima 5300 dv spectrometer. Thermochemical properties were studied via DSC using a PerkinElmer DSC7 calorimeter; it was further used to calculate the ratios of the various phases present using the enthalpy of fusion of tin (7.04 kJ mol^{-1}). Two full DSC cycles were recorded at a constant heating rate of 10 °C min^{-1} from 175 °C to 475 °C and back. "As-prepared" as well as annealed samples were measured.

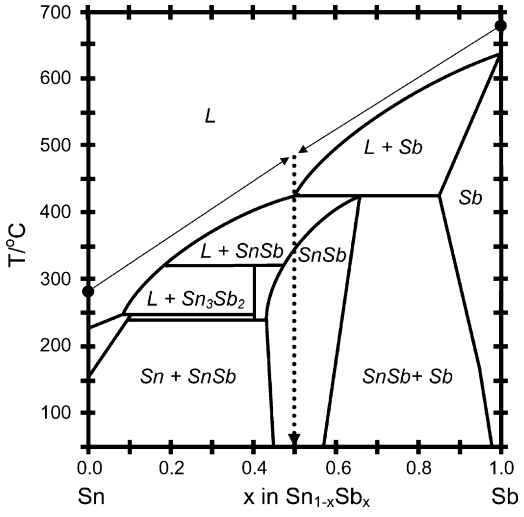

Fig. 1. Phase diagram of $Sn_{1-x}Sb_x$ after Stolen and Gronvold [16]. The closed circles indicate the starting temperature of molten Sn and molten Sb, respectively. The arrows are used as a guide to the eye to show the temperature at which roughly the cooling of the mixture started. The "hourglass" indicates the annealing temperature.

2.3. Electrochemical analysis

Composite electrodes were prepared by mixing 60 wt.% of active material with 20 wt.% of carbon black (CB) (99.9% pure <1 μm from Alfa) and 20 wt.% polyvinylidene fluoride (PVDF) (Solvay) in the solvent *N*-methyl-2-pyrrolidone (NMP) (≥99.0% pure from MERCK). These high amounts of CB and binder were used in order to avoid interference in the electrochemical tests of electrode resistances other than from the material itself. The mixture was homogenised using a planetary ball mill (Fritsch Pulverisette 7) at low speed for 15 min. The paste formed was coated on a copper current collector and dried at 120 °C. From these coatings, 14-mm diameter electrodes were punched out and then dried at 60 °C in a vacuum oven. Coin cells for the electrochemical tests were constructed with the following order: Li|$LiPF_6$, EC, DMC|SnSb, CB, PVDF—here EC and DMC stand for ethylene carbonate and dimethyl carbonate, respectively. The electrolyte is 1 M $LiPF_6$ in a 2:1 weight ratio of EC/DMC. The assembling of the coin cells was done in a glove box under helium atmosphere. The cells were tested in galvanostatic mode at a current density of 110 mA g^{-1} (0.24 mA cm^{-2}) which corresponds roughly to $x = 1$ (in Li_xSnSb) in 2 h, i.e. one lithium per SnSb formula unit in 2 h. The cells were then cycled between 0.2 V and 1.3 V, respectively.

2.4. Post-mortem analysis with TEM

Cells were cycled at the same conditions as mentioned above. One was stopped after one discharge (sample A), the second one was stopped after one complete cycle (one discharge and one charge: sample B), the third one was stopped after 15 complete cycles (sample C), and the last one was stopped after 100 complete cycles (Fig. 6b). After finishing the measurements, the coin cells were opened in a helium filled glove box—the different layers were separated carefully for further analysis. Washing of the electrodes was performed with DMC in an ultrasonic bath in order to remove the lithium salts, which was used in the electrolyte. Then the layers were further rinsed in DMC by centrifugation at 6000 rpm for 1 h. The same procedure was performed twice with NMP instead of DMC, in order to eliminate the binder PVDF. The obtained powders were dried at room temperature under vacuum overnight. It is stressed that all these procedures were performed under helium atmosphere. The dried powders were analysed using TEM on a Philips CM30T electron microscope with a LaB6 filament as electron source operating at 300 kV. For these analyses, samples were mounted on Quantifoil® microgrids (carbon polymer supported by a copper mesh). This was performed by placing a few droplets of a suspension of the initial sample in ethanol on the grid, which then was dried at ambient conditions.

3. Results and discussion

3.1. Composition and morphology

The SEM picture of freshly crushed particles (Fig. 2) shows well-crystallised particles of a few tens of a micrometre, but typically smaller then 45 μm as may be expected by using a 45 μm sieve. These powders were then subject to the following analyses. ICP-OES analysis gave an elemental composition of the powder of around 50 ± 1% for both Sn and Sb as was expected based on the starting composition (Fig. 1). The X-ray diffraction pattern (Fig. 3) shows the presence of two crystalline phases. The most intense peaks arise from intermetallic SnSb. The peaks are quite sharp indicating well-crystallised powders. Crystallites size was calculated using Scherrer formula, the average size was found to be around 75 nm. The second phase was identified as pure metallic tin. The observed sharp

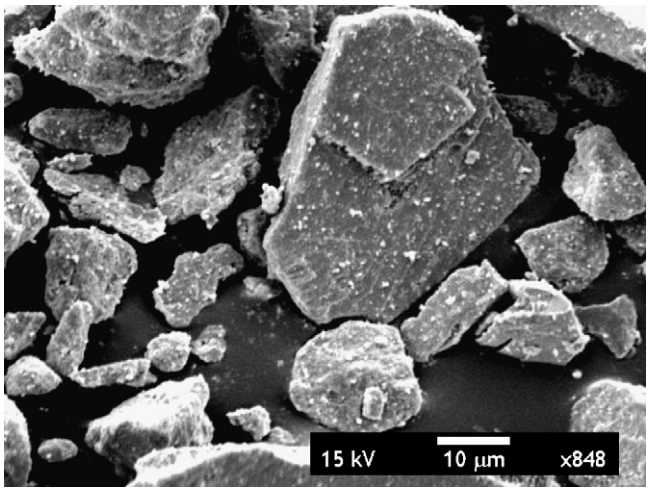

Fig. 2. SEM image of 45 μm-sieved powder of SnSb.

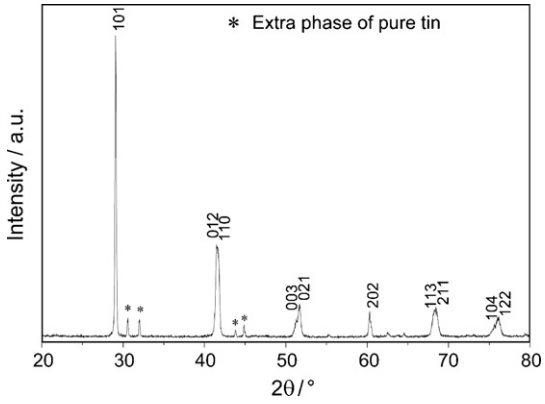

Fig. 3. XRD pattern of SnSb recorded after melting, casting, grinding and sieving. The asterisks indicate pure Sn.

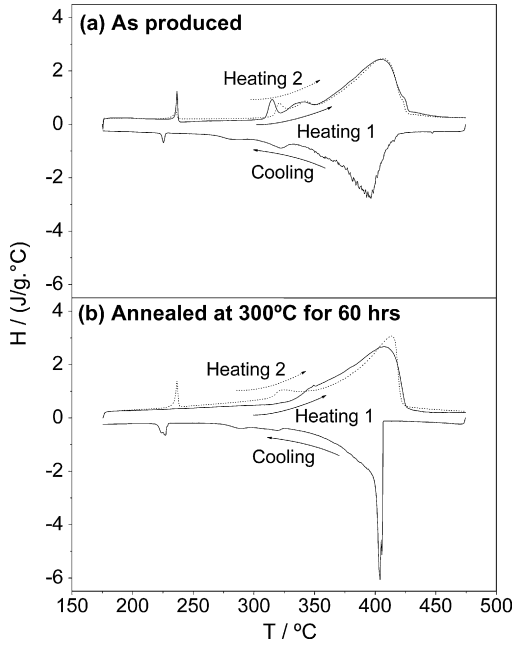

Fig. 4. DSC of SnSb as produced (a) and SnSb annealed at 300 °C for 60 h (b). Scan rate: 10 °C min^{-1}, 175 °C < T < 475 °C.

peaks of this second phase also indicate well-crystallised phase. The DSC analysis (Fig. 4) confirms the presence of two different phases as obtained by XRD. An endothermic peak at 231 °C can be observed during the first heating of the "as-produced" material (Fig. 4a). This peak can easily be attributed to the fusion of a pure tin phase. The area of this peak was calculated in order to obtain the actual value of the enthalpy of fusion of the tin in the material, knowing the value of the enthalpy of fusion per gram of this element (59.3 J g^{-1}), and reporting this to the total mass of the sample. The ratio of the pure tin phase was found to be between 3 wt.% and 5 wt.%. From the annealed sample (Fig. 4b) it is observed that the tin phase has completely disappeared as the peak of fusion at 231 °C is no longer present. However, an exothermic peak is observed at this temperature during the cooling process, and, during the second heat, a fusion peak is observed as well. This demonstrates that a re-crystallisation of a pure tin phase occurs. This experiment shows that the presence of the two phases is not due to the elemental composition which would differ from 1:1, but merely to the kinetics of the cooling process during synthesis.

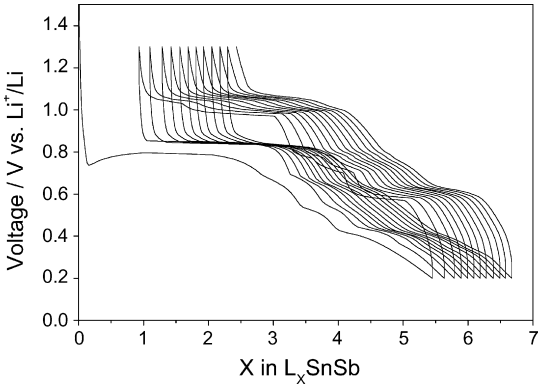

Fig. 5. Voltage profiles of the first 12 cycles of the cell: Li|LiPF$_6$, EC, DMC|SnSb,CB, PVDF. The cell was cycled at i = 55 mA g^{-1} between 0.2 V and 1.3 V.

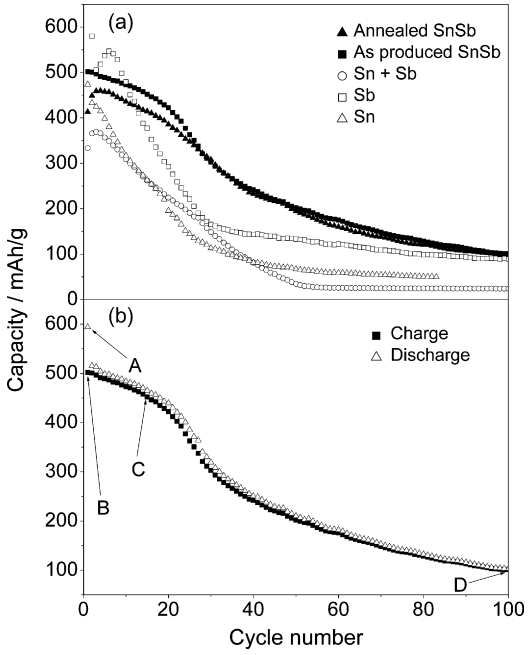

Fig. 6. (a) Charge capacities vs. cycle number curves of the various cells Li|LiPF6, EC, DEM|metal, CB, PVDF, metal is Sn, Sb, Sn + Sn, and SnSb as-prepared as well as annealed. (b) Cycle life of the cell Li|LiPF6, EC, DEM|SnSb, CB, PVDF. At points A, B, C, and D TEM measurements were performed on opened cells.

3.2. Electrochemical analysis

Charge–discharge curves of the "as-produced" samples are presented in Fig. 5. The first discharge differs significantly from the following discharges due to various reasons. Two of these reasons are mentioned here as these are seen as the most important ones for explaining the results. The first one is explained by the existence of oxides usually present at the surface of the powders which lead to an additional reduction giving a sloppy curve in the first part of the discharge. This then is followed by a so-called "negative hump", which is often explained by a metal surface–electrolyte interaction, which can be seen as the formation of a solid electrolyte interface (SEI). This interface grows gradually and leads to a small increase in the impedance, giving rise to a small voltage drop in the discharge curve. After these two phenomena, a first voltage plateau is observed at around 0.8 V, which is generally attributed to Li_3Sb formation [15–17]. Consequently, metallic tin is formed in the mean time according to reaction Eq. (1)

$$SnSb + 3Li \rightarrow Li_3Sb + Sn \quad (1)$$

$$Sn + xLi \rightarrow Li_xSn \quad (2)$$

The following three plateaus then correspond to the different Li_xSn intermetallics phases that are formed by the reaction

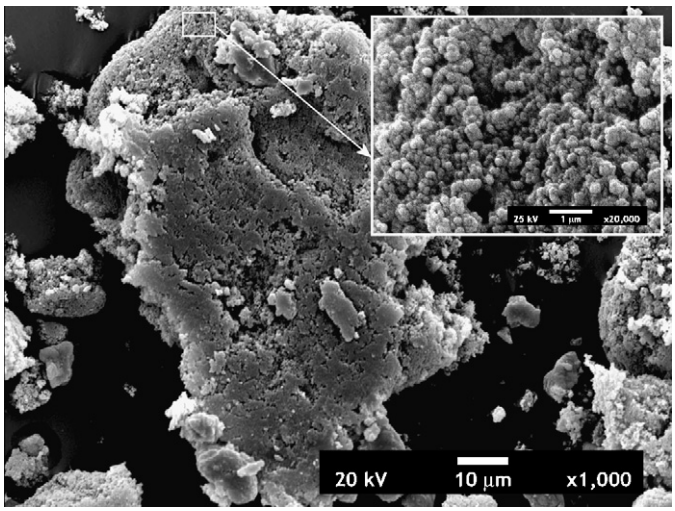

Fig. 7. SEM image of the initial 45 μm-sieved powder of SnSb recorded after charging and discharging. Main image: low magnification (scale bar: 10 μm); top right insert: high magnification (scale bar: 1 μm).

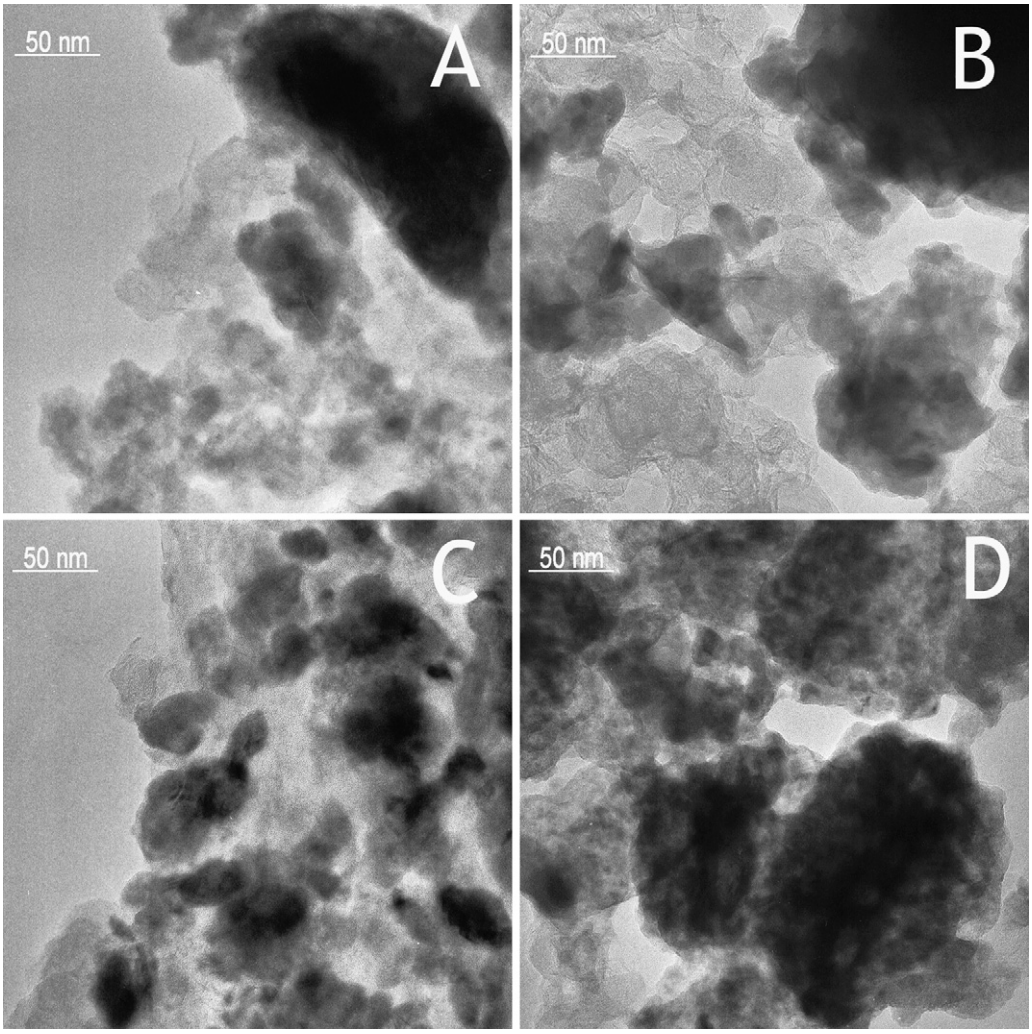

Fig. 8. TEM graphs of cycled electrodes after (A) one discharge (lithiated electrode), (B) one complete cycle (delithiated electrode), (C) 15 completed cycles (delithiated electrode), and (D) 100 completed cycles.

of lithium with tin [15,17,18] (Eq. (2)). According to Fernandez-Madrigal et al. [15] the different inflection points of the curve correspond to the successive formation of Li_3Sb, Li_2Sn_5, LiSn, $Li_{13}Sn_5$, Li_5Sn_2, Li_7Sn_3, Li_7Sn_5 and finally $Li_{22}Sn_5$. During the first charge, the same plateaus can be recognised, except for an extra plateau observed at around 1.05 V. Although this latter voltage plateau is not fully understood, it may be attributed to the formation of the L_2Sb intermetallic phase. The amount of lithium reacting with antimony forming Li_xSb, i.e. near the 0.8 V plateau, is around $x = 2.5$. The total amount of lithium reacted after the first discharge is around $x = 5.5$, which is significantly smaller than the expected theoretical value of $x = 7.4$—here both Li_3Sb and $Li_{22}Sn_5$ are taken into account [15,18,19]. The smaller amount of lithium that has been found to react is attributed to the fact that not all the SnSb reacting with lithium are accessible because of its large particle size. These findings are supported by the fact that during the following cycles, the amount of lithium at the end of each discharge progressively increases towards the theoretical amount of $x = 7.4$. For comparison, in Fig. 6a the cycle lives have been displayed of various cells with different negative electrode materials, i.e. Sb, Sn, a stoichiometric mixture of Sn and Sb, "as-produced" SnSb and annealed SnSb. This figure clearly shows the improved behaviour of either Sn or Sb when using an intermetallic compound, SnSb, with another metal as a buffering matrix Sb or Sn, respectively. The figure further shows that a simple combination of the two metals does not lead to improved capacity. In Fig. 6b, a rather stable capacity upon cycling can be observed with a reasonable fading of around 10% of the capacity after the first 15 cycles. After say 20 cycles, the capacity starts to fade significantly, and this fading continues down to the maximum number of cycles measured. This phenomenon of stable capacity up to 15 cycles followed by a strong fading has been observed with this material made via other methods as well. After 100 cycles the capacity has dropped to 100 mAh g^{-1} where about 825 mAh g^{-1} could be expected theoretically. The source of the fading has been analysed by electron microscopy.

Scanning electron microscopy on charged samples (Fig. 7) shows nano-sizing of the particles as presented in Fig. 2. In Fig. 7 spherical clustered particles of around 20–50 μm are observed.

Transmission electron micrographs are presented in Fig. 8. Here it is observed that nano-particles below 50 nm were formed after one complete lithiation of the material. However, micron-sized particles are still present indicating that not all the SnSb material reacted with lithium after this first cycle. This then explains the low observed capacity in the first cycle. It is also found, that the density or number of the micron-sized particles is decreasing upon further cycling. This is also concordant with the increased capacity upon further cycling found in the charge–discharge curves displayed in Fig. 5. Clearly, by consecutive cycling, a continuous increase in the capacity was observed. This then, can well be understood by a progressively increase of nano-sizing of the material, and thus, an increased access to the still untouched SnSb material. This may be a result of cracking due to volume expansion that then leads to fresher SnSb exposed to the lithium ions in the electrolyte. Besides the increased consumed lithium, an irreversible capacity loss is observed in the Li_xSb (Fig. 6). This capacity fading is due to the formation of the Li–Sb alloys, which seems to form an irreversible intermetallic phase, or a non-accessible phase due to the growth of a solid electrolyte interface. This growing SEI layer then gives rise to a drastic impedance rise leading to capacity fading, a concept that has been reported before [20]. Besides, the nano-sizing of the particles may also result in loss of contact of the active metal component with the current collector via the carbon black. Hence, in this case, electrons are no longer able to arrive at the active metal, and thus the metal becomes inactive with regard to lithium storage.

4. Conclusion

An alternative method for producing the intermetallic SnSb for lithium ion battery negative electrodes was successfully employed. This method, which involves only pure metals as precursors, is rather simple and inexpensive. No special atmosphere was used, as oxidation of the final material was practically not observed. Despite its relative large particle sizes it showed a rather stable capacity for at least 15 cycles. Fading sets in after about 20 cycles and continues for at least 100 cycles. From TEM and electrochemical analyses, this apparent stability was probably caused by two competitive effects, i.e. an irreversible capacity due to an irreversible lithium alloy formation and a yet an unexplored and so fresh part of the alloy that became available by progressively cracking upon further cycling. When all the untouched parts of the alloy would be reached by lithium, this would probably lead to a significant drop of the capacity upon even further cycling. A plausible explanation for the fading observed in that region, is island formation of initial active metal particles that become inactive for lithium storage due to electronic isolation.

Acknowledgements

The authors would like to thank the European Commission for financing part of the work supported via the ALISTORE network of excellence (contract number 503532). Also, the Delft Research Centre for Sustainable Energy SENECU is acknowledged for additional financial support. We would like to give special thanks to Mr. Jan Boomsma from the Delft University of Technology for technical support in the alloy production. SenterNovem is also acknowledged for sponsoring a parallel project that significantly contributed to this work with respect to equipment.

References

[1] R.A. Huggins, Solid State Ionics 113–115 (1998) 57–67.
[2] M. Winter, J.O. Besenhard, Electrochim. Acta 45 (1999) 31–50.
[3] J. Wang, I.D. Raistrick, R.A. Huggins, J. Electrochem. Soc. 133 (1986) 457–460.
[4] K.D. Kepler, J.T. Vaughey, M.M. Thackeray, J. Power Sources 81/82 (1999) 383–387.
[5] C.M. Ionica, P.-E. Lippens, J. Olivier Fourcade, J.-C. Jumas, J. Power Sources 146 (2005) 478–481.
[6] Q.F. Dong, C.Z. Wu, M.G. Jin, Z.C. Huang, M.S. Zheng, J.K. You, Z.G. Lin, Solid State Ionics 167 (2004) 49–54.
[7] D. Larcher, C. Mudalige, A.E. George, V. Porter, M. Gharghouri, J.R. Dahn, Solid State Ionics 122 (1999) 71–83.
[8] H.Y. Lee, S.M. Lee, J. Power Sources 112 (2002) 649–654.
[9] J. Yang, Y. Takeda, N. Imanishi, T. Ichikawa, O. Yamamoto, J. Power Sources 79 (1999) 220–224.
[10] M. Wachtler, M. Winter, J.O. Besenhard, J. Power Sources 105 (2002) 151–160.
[11] H. Li, G. Zhu, X. Huang, L. Chen, J. Mater. Chem. 10 (2000) 693–696.
[12] A. Trifonova, M. Wachtler, M.R. Wagner, H. Schroettner, Ch. Mitterbauer, F. Hofer, K.-C. Moller, M. Winter, J.O. Besenhard, Solid State Ionics 168 (2004) 51–59.
[13] J. Yang, Y. Takeda, N. Imanishi, T. Ichikawa, O. Yamamoto, Solid State Ionics 135 (2000) 175–180.
[14] J. Yin, M. Wada, S. Tanase, T. Sakai, J. Electrochem. Soc. 151 (2004) A867–A872.
[15] F.J. Fernandez-Madrigal, P. Lavela, C.P. Vicente, J.L. Tirado, J.C. Jumas, J. Olivier-Fourcade, Chem. Mater. 14 (2002) 2962–2968.
[16] S. Stolen, F. Gronvold, J. Chem. Thermodyn. 31 (1999) 379–398.
[17] H. Zhao, C. Yin, H. Guo, W. Qiu, Electrochem. Solid-State Lett. 9 (2006) A281–A284.
[18] L. Aldon, A. Garcia, J. Olivier-Fourcade, J.-C. Jumas, F.J. Fernandez-Madrigal, P. Lavela, C. Perez Vicente, J.L. Tirado, J. Power Sources 119–121 (2003) 585–590.
[19] R.A. Huggins, J. Power Sources 81/82 (1999) 13–19.
[20] J. Yang, Y. Takeda, N. Imanishi, O. Yamamoto, J. Electrochem. Soc. 146 (1999) 4009–4013.